

Dynamic spatiotemporal modeling of a habitat defining plant species to support wildlife management at regional scales

ANDREW T. TREDENNICK^{*1,2}, THOMAS PREBYL¹, ADRIAN P. MONROE³, JOHN LOMBARDI¹, &

4 CAMERON L. ALDRIDGE⁴

⁵ *¹Western EcoSystems Technology, Inc., Laramie, WY*

²*Center for the Ecology of Infectious Diseases, University of Georgia, Athens, GA*

⁷³*Fort Collins Science Center, U.S. Geological Survey, Fort Collins, CO*

⁴Natural Resource Ecology Laboratory and Department of Ecosystem Science and Sustainability,
Colorado State University, Fort Collins, CO, in cooperation with US Geological Survey, Fort Collins

11 Open Research Statement

¹² Data and code are provided as private-for-peer review (shared publicly in a repository: <https://github.com/atredennick/sagecastR>). Data and code will be archived on Zenodo upon acceptance.

*Corresponding author: email, atredennick@west-inc.com; phone, 307-721-7343

14 **Abstract**

15 Sagebrush (*Artemisia* spp.) ecosystems provide critical habitat for the near-threatened Greater
16 sage-grouse (*Centrocercus urophasianus*). Thus, future loss of sagebrush habitat because of land
17 use change and global climate change is of concern. Here we use a dynamic additive spatio-
18 temporal model to estimate the effects of climate on sagebrush cover dynamics at 32 sage-grouse
19 management areas in Wyoming. We use the fitted models to quantify the sensitivity of each man-
20 agement area to precipitation and temperature, and to make probabilistic projections of sagebrush
21 cover from present to 2100 under three climate change scenarios. Global circulation models pre-
22 dict an increase in temperature and no change in precipitation for Wyoming. Sensitivity to climate
23 varied among management areas but the most common response (70% of management areas) was
24 a positive effect of temperature on sagebrush performance. The combination of positive sensitiv-
25 ity to temperature and the predicted increase in temperature under all climate change scenarios
26 resulted in projections of increased sagebrush cover for most management areas. We character-
27 ized management areas as “optimal” or “suboptimal” based on the percentage of grid cells in each
28 management area with sagebrush cover exceeding a nesting habitat target value. Only 18% of
29 management areas are projected to switch from being currently optimal to suboptimal in the fu-
30 ture. Thirty-five percent of management areas are projected to switch from being suboptimal to
31 optimal. The most common outcome (47%) was for currently suboptimal management areas to
32 remain suboptimal, even though average cover tended to increase in those areas. The direct effects
33 of climate change appear to favor sagebrush performance in the future for most sage-grouse core
34 areas in Wyoming. Our approach is broadly applicable to quantitative climate change assessments
35 where remotely-sensed estimates of habitat-defining vegetation are available.

36 *Key words:* Artemisia, *Centrocercus urophasianus*, *climate change*, *Greater sage-grouse*, *pop-*
37 *ulation model*, *remote sensing*, *sagebrush*

³⁸ Introduction

³⁹ Environmental management and stewardship requires assessing tradeoffs (Walters and Hilborn
⁴⁰ 1978, Farber et al. 2006). For example, land managers must consider the long-term impacts of
⁴¹ climate change and the near-term impacts of ecosystem degradation (e.g., Nepstad et al. 2008).
⁴² Because populations, communities, and ecosystems are not static, using the current status of an
⁴³ ecosystem to make management decisions may not be optimal (Boettiger et al. 2016). A better
⁴⁴ approach is to consider the past, current, and future status of ecosystems. Doing so requires pro-
⁴⁵ jections of how an ecosystem might respond to future stressors and conditions (Clark et al. 2001,
⁴⁶ Dietze et al. 2018).

⁴⁷ Infrastructure development indirectly and negatively affects species through habitat loss and
⁴⁸ transformation, which is a major driver of biodiversity loss (Sala et al. 2000, Cardinale et al.
⁴⁹ 2012, Powers and Jetz 2019). Wildlife management often requires assessing tradeoffs between the
⁵⁰ benefits of development and the costs of habitat loss or degradation (McShane et al. 2011). To
⁵¹ assess that tradeoff, managers often identify areas of high and low quality habitat. Low quality
⁵² habitat is then preferred for habitat alteration. But habitat quality is not static and global climate
⁵³ change has the potential alter the trajectory of an ecosystem. Some currently high quality habitat
⁵⁴ (for a particular species) might quickly change if on a range edge while lower quality habitat in
⁵⁵ the middle of the range might maintain its general structure and function longer (Amburgey et al.
⁵⁶ 2018). Habitat on the edge of an ecosystem's range might also improve. For example, warming
⁵⁷ temperatures could benefit some plants at the cold edge of their range (Kleinhesselink and Adler
⁵⁸ 2018). Thus, climate change adds a new dimension to habitat assessments, where we are not only
⁵⁹ concerned about the current status of habitat but also what that habitat might look like 30 to 100
⁶⁰ years in the future.

⁶¹ Land management in the western United States focuses on several uses and species, but Greater
⁶² sage-grouse (*Centrocercus urophasianus*, hereafter “sage-grouse”) typically drive the conversa-
⁶³ tion in sagebrush dominated ecosystems. Sage-grouse are a protected species in Canada (Species
⁶⁴ at Risk Act [S.C. 2002, c. 29], <https://laws-lois.justice.gc.ca/eng/acts/S-15.3/>) and are listed as

65 “warranted, but precluded” for listing under the United States Endangered Species Act of 1973
66 (U.S. Fish and Wildlife Service [USFWS] 2010). Sagebrush ecosystems provide critical habitat for
67 Greater sage-grouse and other sagebrush obligate species (Carlisle and Chalfoun 2020). Conserva-
68 tion of sagebrush ecosystems is primarily aimed at keeping sage-grouse off the endangered species
69 list but sagebrush conservation will benefit other species, too (Rowland et al. 2006, Smith et al.
70 2019, Pilliod et al. 2020). In response to declining sage-grouse populations, the Wyoming Game
71 and Fish Department has delineated 32 sage-grouse core areas, covering approximately 15 million
72 acres of sage-grouse habitat (State of Wyoming 2015). The stated goal of the Core Area strategy
73 is “...to minimize future disturbance by co-locating proposed disturbances within area already
74 disturbed or naturally unsuitable” (State of Wyoming 2015). Sage-grouse populations are active
75 in all core areas and most maintain stable populations (Edmunds et al. 2018), though populations
76 outside of these core areas are not performing the same.

77 In Wyoming, many of the landscapes with the highest potential for wind energy also support
78 critical sage-grouse habitat in the form of sagebrush dominated ecosystems. This presents a chal-
79 lenge to land management: Should land be prioritized for sage-grouse conservation or renewable
80 energy development? Renewable energy infrastructure that can mitigate the impacts of climate
81 change could benefit sage-grouse in the long run. Therefore, it is critical to understand the poten-
82 tial impacts of climate change across sagebrush landscapes because some areas may become less
83 beneficial to sage-grouse due to climate change, making those areas attractive for development of
84 renewable energy infrastructure, potentially minimizing such conflicts. Considering how climate
85 change impacts whether a sage-grouse core area is or will be “naturally unsuitable” clearly falls
86 within the scope of the Core Area strategy. More broadly, assessing current and future habitat
87 suitability *vis-a-vis* species of concern is essential as we face difficult and inevitable trade-offs
88 between land preservation and land-use to combat climate change.

89 The sagebrush biome, as a whole, is in peril (Palmquist et al. 2021). But Wyoming is thought to
90 be a stronghold where sagebrush will persist and possibly thrive in the future, especially compared
91 to other parts of its range (Palmquist et al. 2021). In part, this is because the sagebrush biome

92 in Wyoming has been less susceptible to cheatgrass (*Bromus tectorum*) invasion, compared to
93 other parts of the sagebrush biome (Pastick et al. 2021). Cheatgrass invasion, and the subsequent
94 cheatgrass-fire feedback cycle, is the main driver of the loss of sagebrush cover across most of
95 sagebrush's range (Balch et al. 2013). Because susceptibility to cheatgrass invasion is an indirect
96 effect of climate change (Chambers et al. 2007, Bradley 2009), and because cheatgrass invasion
97 has not been as dramatic in Wyoming, it stands to reason that the direct effects of climate change
98 have important implications in Wyoming. This is especially true if increases in sagebrush cover due
99 to climate change can inhibit cheatgrass invasion. Indeed, recent modeling suggests that warming
100 temperatures will benefit sagebrush more than cheatgrass at high elevation sites, assuming fire is
101 limited (Palmquist et al. 2021). Therefore, this paper focuses on modeling the direct effects of
102 climate on sagebrush cover change.

103 Here we describe a computationally efficient Bayesian spatiotemporal modeling approach for
104 making probabilistic projections of sagebrush cover dynamics under the direct effects of climate
105 change in Wyoming, USA using remotely sensed cover estimates. A key feature of our approach is
106 using the probabilistic projections to evaluate specific management targets for sagebrush cover in
107 sage-grouse core areas. Our approach is applicable to diverse situations where clear management
108 targets exist and spatiotemporal data are available to train probabilistic models.

109 Materials and Methods

110 Data

111 Remotely-sensed time series

112 We used the Rangeland Condition, Monitoring, Assessment, and Projection (RCMAP) data prod-
113 uct from the National Land Cover Database (NLCD), a product of the Multi-Resolution Land
114 Characteristics Consortium (Rigge et al. 2020). We downloaded the “NLCD BIT Sagebrush Frac-
115 tional Component” estimates for each year from 1985 to 2018, subset the data to the Wyoming

¹¹⁶ Sage-grouse core areas, and then resampled the data up to 100-meter resolution using the mean to
¹¹⁷ aggregate cover across 30-meter grid cells. We resampled the data to make the analysis computa-
¹¹⁸ tionally tractable: decreasing the spatial resolution resulted in fewer cells of data per year and thus
¹¹⁹ reduced the total size of the observed data. Time series of cover are shown in Fig. 1. There are no
¹²⁰ data for 2012, which we handled naively by letting 2011 be the “lag cover year” for 2013.

¹²¹ [Figure 1 about here.]

¹²² Climate covariates

¹²³ We downloaded historical climate estimates from PRISM (<http://prism.oregonstate.edu/>), with spa-
¹²⁴ tial extents that matched the sage-grouse core areas. From these estimates, we calculated two
¹²⁵ climate covariates: 1) average spring-through-summer temperature and 2) average spring-through-
¹²⁶ summer precipitation. We defined spring-through-summer as March 1 through August 31 for each
¹²⁷ year. We decided on the two covariates based on our previous work (Tredennick et al. 2016) and
¹²⁸ more recent work by Kleinhesselink and Adler (2018). Previous modeling of sagebrush dynamics
¹²⁹ in Wyoming and across the sagebrush range used “lagged covariates” like precipitation in the year
¹³⁰ prior to an observed transition. We do not use lagged covariates here because exploratory work
¹³¹ suggests that lagged covariates result in correlated and confounded parameter estimates (Kleinhes-
¹³² selink pers. comm.).

¹³³ Climate projections

¹³⁴ We used climate projections from Global Circulation Models (GCMs) that contributed to the
¹³⁵ CMIP6 project (Eyring et al. 2016). Groups that contributed to CMIP6 provided output from
¹³⁶ several experimental conditions. We used three common experimental conditions for generating
¹³⁷ future projections under different shared socio-economic pathways (SSPs): ssp126 (low future
¹³⁸ carbon emissions), ssp245 (intermediate future carbon emissions), and ssp585 (high future car-
¹³⁹ bon emissions) (see Eyring et al. (2016) for more details). GCM ouputs were downloaded from
¹⁴⁰ Lawrence Livermore National Library archives of CMIP6 model simulations and projections. We

141 used the `esfg_query` function from the `epwshiftr` R package (Jia and Chong 2020) to query the
 142 database and download the data. In total, we compiled future climate projections from 18 GCMs.
 143 We applied a bias correction to the GCM values by shifting the means of GCM projections in
 144 reference to PRISM data from the historical time period.

145 GCM projections vary in their accuracy depending on location. Therefore, we weighted each
 146 of the GCMs by their ability to reproduce observed data (Rupp et al. 2013). To evaluate each
 147 GCM we compared historical projections (1985 - 2018) from each GCM to PRISM data for the
 148 same time span and geographic area. For each year we resampled the historic GCM raster data to
 149 match the spatial resolution of the PRISM data and extracted values for the two climate variables
 150 (average spring-through-summer temperature and average spring-through-summer precipitation)
 151 for each sage-grouse core area, then calculated the mean climate variable value across all core
 152 areas.

153 Following Rupp et al. (2013), we calculated the relative error (E^*) across the entire time span
 154 for both climate variables and for each GCM as

$$E_{i,j}^* = \frac{E_{i,j} - \min(E_j)}{\max(E_j) - \min(E_j)} \quad (1)$$

155 where i indexes the variable (temperature or precipitation) and j indexes the GCM. $E_{i,j}$ is the mean
 156 absolute error, calculated as $E_{i,j} = \frac{\sum_{k=1}^K |x_{i,j,k} - z_{i,j,k}|}{K}$, where x is the observed value from PRISM and
 157 z is the value from the GCM and k indexes the observation (an annual mean value for a particular
 158 year), and K is the total number of observations. Last, we averaged the E^* values across the two
 159 variables (temperature and precipitation) to arrive at a single relative error value for each of the J
 160 GCMs: $E_j^* = (\sum_{i=1}^N E_{i,j}^*) / N$, where $N = 2$ is the total number of variables. The resulting relative
 161 errors for each GCM were used as weights ($w_j = 1 - E_j^*$) when making projections of sagebrush
 162 dynamics forced by the GCM output. Specifically, the projected time series of weather we used
 163 under each scenario is the weighted average of all GCMs, with w_j being the weight for each GCM
 164 j .

165 **Model**

166 **Dynamic additive spatio-temporal model for sagebrush cover**

167 We used a descriptive, dynamic model of sagebrush cover, building on our previous work (Tre-
168 dennick et al. 2016) and animal population modeling described by Conn et al. (2015). Our model
169 represents the observed sagebrush cover in cell i of year t ($y_{i,t}$) as arising from a Poisson process
170 with rate $\exp(\mu_{i,t})$:

$$y_{i,t} \sim \text{Poisson}(\exp(\mu_{i,t})). \quad (2)$$

171 The deterministic process model follows the log-transformed version of a Gompertz population
172 growth model, representing $\mu_{i,t}$ as

$$\mu_{i,t} = \beta x'_{i,t} + \gamma_t + w_i \quad (3)$$

173 where β is a vector of regression coefficients, $x_{i,t}$ is a vector of covariates for cell i at time t , γ_t is a
174 temporal random effect, and w_i is a spatial offset for each cell i . The covariate vector $x_{i,t}$ is one row
175 of the design matrix \mathbf{X} , which includes a column of 1s for the intercept, a column of logged lag
176 cover ($\log(y_{t-1})$) values, a column for the precipitation covariate, and a column for the temperature
177 covariate. \mathbf{X} is a $n \times p$ matrix and each row represents a single observation, indexed by time (t ,
178 year of observation) and cell (i , spatial location). We added a small offset (0.0001) to all one-year
179 lagged observed percent cover values that occur in the design matrix \mathbf{X} before logging those values
180 so that 0 cover values could be included easily.

181 In previous work we estimated the spatial offset using kernel convolution and dimension re-
182 duction (Tredennick et al. 2016). Estimating the spatial offset is not strictly necessary because the
183 data represent a full sample of the spatial domain. Here we use an empirical approach to calculate
184 the spatial offset because it substantially reduces computational time and results in a better repre-
185 sentation of the spatial variance. We calculated the spatial offset for each grid cell as the difference
186 between the log of the focal mean of a cell over time and the log of mean cover across each com-

187 plete core area over time. More specifically, we calculated the spatial offset w_i for each cell i in a
188 core area as

$$w_i = \log(\bar{f}_i) - \log(\bar{y}), \quad (4)$$

189 where \bar{y} is the mean cover across all years and cells within the core area and \bar{f}_i is the weighted
190 focal mean of all surrounding cells within a radius r ,

$$\bar{f}_i = \frac{1}{n} \sum_{j=1}^n x_j \times k_j, \quad (5)$$

191 with weights, k_j , defined using an exponential decay function,

$$k_j = \exp\left(\frac{-d_j}{(r \times \frac{1}{3})}\right), \quad (6)$$

192 where d_j is the distance in meters from cell j to focal cell i and n is the total number of cells
193 within the radius r of the focal cell. We defined r as the maximum range of spatial dependence
194 in residuals from a simple generalized linear model (GLM) fit without climate covariates for each
195 core area (Tredennick et al. 2016). The **focal** function from the **raster** package in R cannot
196 accommodate missing values when calculating a focal mean with custom weights. We pre-filled
197 any cells with missing cover values using a focal mean with equal weight for all cells within the
198 analysis radius r . After calculating \bar{f}_i , all cells that originally had missing cover values were re-set
199 to NA before calculating the final spatial offset value w_i . Missing cover values corresponded to
200 masked areas not defined as “sagebrush” habitat in the RCMA products.

201 The full Bayesian posterior distribution of the dynamic-additive spatiotemporal model is:

$$\begin{aligned}
[\beta, \gamma, \sigma_\gamma | \mathbf{y}, \mathbf{X}, \mathbf{w}] &\propto \prod_{t=1}^T \prod_{i=1}^N [y_{i,t} | \beta, \gamma, w_i] \\
&\times [\gamma_t | \sigma_\gamma] \\
&\times [\beta] [\sigma_\gamma]. \tag{7}
\end{aligned}$$

202 An attractive feature of the Gompertz population model in log space (Eq. 3) is that equi-
 203 librium abundance is defined as: $\mu' = \beta_1 / (1 - \beta_2)$ (Ives et al. 2003, Kleinhesselink and Adler
 204 2018). Note that this definition holds when the random effects are centered on 0 and when the
 205 covariates are scaled and centered on 0. Both of these conditions hold in our model. We use
 206 equilibrium abundance (cover, in our case) as a starting point for sensitivity analyses. For ex-
 207 ample, equilibrium cover across all cells in a core area is $\bar{y}' = \exp(\mu')$. Equilibrium cover for
 208 a particular cell (i) is $y'_i = \exp(\mu' + w_i)$. Equilibrium cover for a particular cell (i) under a cli-
 209 mate scenario where the future climate is 1 standard deviation greater than current climate is
 210 $y'_i = \exp(\mu' + w_i + (1 \times \beta_3) + (1 \times \beta_4))$ (Kleinhesselink and Adler 2018). Projections of future
 211 cover were initialized with observed cover in 2018.

212 We used results from Tredennick et al. (2016) to define informative prior distributions for the
 213 intercept (β_1) and density-dependence (β_2) regression parameters in Eq. 3 (Table 1). Vague prior
 214 distributions were assigned to all other parameters (Table 1).

215 [Table 1 about here.]

216 Model fitting and evaluation

217 We used Hamiltonian Monte Carlo (HMC) to approximate the posterior distributions of all un-
 218 known parameters. Specifically, we used the Stan software (Stan Development Team 2020) to
 219 implement the HMC algorithm, using the rstan package (Guo et al. 2020) to connect Stan to R. We
 220 ran three chains of 1,000 iterations after a burn-in of 1,000 iterations. Convergence of the MCMC
 221 chains was assessed visually with traceplots and by ensuring that the 95% upper credible interval

222 of scale reduction factors (\hat{R}) were less than 1.1 (Gelman and Rubin 1992, Gelman and Hill 2006).
 223 Convergence diagnostics for the intercept (β_1) and the temporal random effects (γ) were computed
 224 after applying “post-sweeping” to address mixing and convergence problems associated with weak
 225 identifiability (Ogle and Barber 2020).

226 We used a subset of the data to fit the model. We did this to make estimation via MCMC
 227 possible in a reasonable time frame. We extracted a spatially balanced 5% sample of grid cells
 228 from each core area to use for model fitting. We used the function `bas.polygon` from the **SDraw**
 229 R package (McDonald et al. 2020) to sample the grid cells for model fitting. Some core areas
 230 (e.g., Greater South Pass) were divided into smaller subsets that were fitted independently due to
 231 memory constraints. Core areas that were divided are indicated by having a number next to their
 232 name or abbreviation (e.g., Greater South Pass 1, Greater South Pass 2, etc.). Note that the spatial
 233 offsets for each grid cell i (w_i) were calculated for the entire spatial domain and then we extracted
 234 the 5% sample of all relevant information: cover, lag cover, climate covariates, and the spatial
 235 effects for each selected grid cell.

236 We used posterior predictive checks to calculate Bayesian P values assessing the lack-of-fit
 237 between the model and the data (Hobbs and Hooten 2015, Conn et al. 2018). We simulated
 238 cover data for each cell and year ($y_{i,t}^{\text{new}}$) from the model at each MCMC iteration and used a chi-
 239 square statistic to compare the data (both original and “new” data) to the expected values from
 240 the deterministic regression model. The test statistics were then summed over time and space
 241 separately, yielding test statistics for each cell over years for both the new and original datasets,

$$\tau_i^{\text{new}} = \sum_{t=1}^Y \frac{(y_{i,t}^{\text{new}} - \mu_{i,t})^2}{\mu_{i,t}} \quad (8)$$

242 and

$$\tau_i = \sum_{t=1}^Y \frac{(y_{i,t} - \mu_{i,t})^2}{\mu_{i,t}}, \quad (9)$$

243 and for each year over cells for both the original and new datasets,

$$\tau_t^{\text{new}} = \sum_{i=1}^S \frac{(y_{i,t}^{\text{new}} - \mu_{i,t})^2}{\mu_{i,t}} \quad (10)$$

²⁴⁴ and,

$$\tau_t = \sum_{i=1}^S \frac{(y_{i,t} - \mu_{i,t})^2}{\mu_{i,t}}. \quad (11)$$

²⁴⁵ We then computed Bayesian p-values as the proportion of the total number of MCMC iterations for
²⁴⁶ which $\tau^{\text{new}} > \tau$ for each cell or year. Lastly, we average the Bayesian p-values over years and cells
²⁴⁷ to compute two final p-values to evaluate lack-of-fit: one for lack-of-fit over the spatial dimension
²⁴⁸ (P_B^{space} , averaged over years) and one for lack-of-fit over the temporal dimension (P_B^{time} , averaged
²⁴⁹ over cells). Posterior predictive checks were done using a new spatially balanced sample of the data
²⁵⁰ (i.e., a different sample than used to fit the model).

²⁵¹ All computations were done in R (R Core Team 2020). We bundled the computer code needed
²⁵² to format data, fit the model, evaluate the model, and project the model forward in an R package
²⁵³ called **sageCastR** (<http://lar-git.west-inc.com/atredennick/sagecastr>). Note that the R package is
²⁵⁴ not a generalizable piece of software; it is a code bundle for this particular project. We also note
²⁵⁵ that fitting the models required a high memory machine and parallel processing. Interested users
²⁵⁶ can modify the code for future research.

²⁵⁷ Model projections

²⁵⁸ We made projections of sagebrush cover in each core area under each of the three climate change
²⁵⁹ scenarios (ssp126, ssp245, and ssp585). Initial conditions were defined as the last year of BIT
²⁶⁰ cover estimates for each core area. Climate covariates for each year were calculated as the weighted
²⁶¹ averages across the GCMs. The weighted averages for the precipitation and temperature covariates
²⁶² were then scaled using the mean and standard deviation for each covariate from the model fitting
²⁶³ stage. This was done independently for each core area and was necessary because we used Z-score
²⁶⁴ transformed covariates for model fitting. We projected sagebrush cover to the year 2100, using

265 50 random MCMC parameter sets to approximate the posterior predictive distribution (Hobbs and
266 Hooten 2015). We used 50 posterior parameter sets instead of the full posterior distribution (3000
267 MCMC parameter sets) to decrease computation time and data storage.

268 We also used a colonization model when projecting the model forward to avoid local extinction
269 in grid cells. We fit a binomial regression model for each core area to estimate the probability of a
270 grid cell with zero percent cover in year t transitioning to non-zero cover in year $t+1$ (Tredennick et
271 al. 2016). This probability was used in the dynamic projections whenever a grid cell had zero cover
272 to simulate whether the grid cell would stay at zero or increase to non-zero cover. We calculated
273 the average cover in cells that transitioned from zero cover to non-zero cover for each core area.
274 Those values were used in the simulation model as the cover assigned to cells that were simulated
275 to transition from zero cover to non-zero cover.

276 Our main goal was to evaluate future cover projections relative to specific management targets.
277 We defined two management targets: 1) the percent cover needed at 100-meter resolution to main-
278 tain sage-grouse nesting habitat and 2) the percent cover needed at 100-meter resolution to maintain
279 sage-grouse summer habitat. We used the 1985-2018 sagebrush cover rasters (resampled to 100 m
280 resolution) to determine the 95% quantile of the time series for each pixel. This quantile should in-
281 dicate potential sagebrush cover at each pixel while reducing the influence of temporal anomalies.
282 Then, we divided Wyoming into three regions (southwest, central, and northeast) and determined
283 the median value across all 95% quantiles that intersected either nesting or summer sage-grouse
284 habitat, by region (Fedy et al. 2014). These provided threshold values for nesting and summer
285 habitat that were region-specific yet consistent with thresholds recommended by the Sage-grouse
286 Habitat Assessment Framework: 15-25% cover for nesting and 10-25% cover for summer (Stiver
287 et al. 2015). The threshold values we calculated are provided in the online supporting information.

288 Based on Fedy et al. (2014), we set our landscape level management goal to be 50% of grid
289 cells in a core area meeting or exceeding the nesting target percent cover value. We defined core
290 areas as “optimal” or “suboptimal” for sage-grouse based on this management goal: optimal =
291 50% of grid cells meeting or exceeding the nesting target, suboptimal = 50% of grid cells below

292 the nesting target. We further categorized core areas into four groups: 1) areas that were estimated
293 to be optimal in 2019 and are projected to remain optimal by 2100, 2) areas that were estimated to
294 be optimal in 2019 and are projected to become suboptimal by 2100, 3) areas that were estimated
295 to be suboptimal in 2019 and are projected to become optimal by 2100, and 4) areas that were
296 estimated to be suboptimal in 2019 and are projected to remain suboptimal by 2100. Categorization
297 was done assuming the ssp585 climate forcing scenario because observed emissions have most
298 closely followed the modeled emissions of ssp585's precursor (RCP8.5) in the recent past. We
299 used the 2019 model projections as the baseline for categorization rather than observed cover in
300 2018 because the projections have slightly lower spatial variance than the observed data. We used
301 sage-grouse population growth rate estimates from Edmunds et al. (2018) to see whether core
302 areas projected to become optimal or suboptimal have currently declining, stable, or increasing
303 sage-grouse populations.

304 **Predicting sensitivity classification**

305 We sought to predict the variation of precipitation and temperature sensitivities across core areas
306 based on soil conditions, elevation, mean annual precipitation, and mean annual temperature. We
307 did this as a second-step after fitting the models above because the focus of our modeling was on
308 predictions for each core area, rather than inference on why a core area was responding in a certain
309 way. However, we did want to explore possible influences on sensitivities, if possible.

310 We fit logistic regression models independently for temperature and precipitation sensitivities af-
311 ter classifying the responses as negative or positive. Forty-seven covariates were included. Eleven
312 soil properties from POLARIS (Chaney et al. 2019) were used for each core area, quantified as
313 the mean, median, 5th percentile, and 95th percentile statistics across six depths. We averaged
314 the metrics across depths to arrive at $11 \times 4 = 44$ soil property covariates and three additional
315 covariates: mean annual precipitation (from PRISM 30-year normals, 1981-2010), mean annual
316 temperature (from PRISM 30-year normals, 1981-2010), and elevation (from USGS North Amer-
317 ica digital elevation map). All covariates were averaged over the grid cells in each core area. We

318 used least-absolute shrinkage (LASSO) regression to perform model selection and identify the best
319 predictor variables. Models were fit in Python (Van Rossum and Drake 2009) using scikit-learn
320 (Pedregosa et al. 2011) libraries and routines.

321 Results

322 Global circulation model rankings and projections

323 Relative errors of the GCMs showed that no single GCM was best at recreating historic temperature
324 and precipitation (Fig. 2A). The best GCM was INM-CM4-8, which had the lowest combined
325 relative error for precipitation and temperature (Fig. 2). The errors in the “Combined” panel are
326 inversely proportional to the weights used when aggregating projections of sagebrush dynamics
327 in the future. Projections based on the INM-CM4-8 future climate covariates will have the most
328 weight and projections based on the SAMO-UNICON model will have the least weight.

329 The amount of spring-through-summer precipitation is not expected to change in Wyoming,
330 according to the GCMs we evaluated (Fig. 2B). Temperature is projected to increase, with the
331 largest increase expected under the ssp585 emissions scenario (Fig. 2B). Average temperature in
332 2080-2100 is projected to be 6.7 degrees Celsius higher than average temperature from 1982-2015
333 under the ssp585 emissions scenario (Table 2). Interannual variation is not expected to substantially
334 increase or decrease over time (Table 2).

335 [Table 2 about here.]

336 [Figure 2 about here.]

337 Statistical model evaluation

338 Convergence diagnostics indicated that all MCMC chains converged on their stationary distribu-
339 tions (upper 0.95 quantiles of $\hat{R} < 1.1$ for all parameters; see online supporting information). Most
340 Bayesian P -values indicated no lack-of-fit because they were greater than 0.05 and less than 0.95

³⁴¹ for both the spatial (P_B^{space}) and temporal (P_B^{time}) test statistic P -values. The P_B^{time} value for Elk
³⁴² Basin West indicated lack-of-fit. The P_B^{space} values for Powder, Sage, Seedskadee, and Uinta indi-
³⁴³ cated lack-of-fit. We do not present any further results on these sites because inference from their
³⁴⁴ models cannot be trusted (Hobbs and Hooten 2015).

³⁴⁵ **Parameter estimates**

³⁴⁶ Posterior distributions for all model parameters for each core area are presented in the online
³⁴⁷ supporting information. The posterior distributions of equilibrium cover ($y' = e^{\beta_1/(1-\beta_2)}$) for
³⁴⁸ each core area contain the observed mean cover values, except for a few core areas (Fig. 3).
³⁴⁹ Cases where mean observed cover does not fall within estimated equilibrium cover suggest that
³⁵⁰ climate effects over the past 30 years or other disturbances not modeled (but potentially reflected in
³⁵¹ random year effects) have kept cover from reaching the equilibrium. Climate effects are described
³⁵² as sensitivities below.

³⁵³ [Figure 3 about here.]

³⁵⁴ [Table 3 about here.]

³⁵⁵ **Sensitivities**

³⁵⁶ All core areas showed some sensitivity to climate drivers (Fig. 4). The majority of core areas had
³⁵⁷ a positive sensitivity to temperature and negative sensitivity to precipitation ($n = 16$; Fig. 5). The
³⁵⁸ most consistent pattern was a positive effect of temperature on sagebrush performance ($n = 24$ out
³⁵⁹ of 34 total [70%]; Figs. 4, 5).

³⁶⁰ [Figure 4 about here.]

³⁶¹ [Figure 5 about here.]

³⁶² Averaging over all the posterior distributions for the precipitation and temperature effects, we
³⁶³ found that overall average effect of precipitation was negative: mean = -0.036 (pseudo 95% BCI

³⁶⁴ = -0.038, -0.034). The overall average effect of temperature was positive: mean = 0.025 (pseudo
³⁶⁵ 95% BCI = 0.023, 0.027). Note that we refer to the confidence intervals as “pseudo BCIs” because
³⁶⁶ the average of the posteriors is not strictly the cross-core area posterior distribution. Nonetheless,
³⁶⁷ the average values do inform the general pattern. The variance of the overall average effects should
³⁶⁸ be viewed as the variance of the mean effect, not as the variance of effect sizes across core areas.

³⁶⁹ Projections

³⁷⁰ Projections of sagebrush cover into the future are primarily driven by the sensitivity of cover to
³⁷¹ temperature and the magnitude of temperature change. This is because precipitation is not pro-
³⁷² jected to increase or decrease much in the future in Wyoming (Fig. 2B). Because most core areas
³⁷³ had a positive sensitivity to temperature, sagebrush cover is projected to increase at most core areas
³⁷⁴ (Fig. 6). Projections of sagebrush cover are similar across GCM scenarios until about mid-century,
³⁷⁵ at which point ssp585 projections diverge if temperature has a large (positive or negative) effect on
³⁷⁶ interannual changes in sagebrush cover (Fig. 6).

³⁷⁷ More core areas were projected to increase ($n = 21$ for ssp126; $n = 22$ for ssp245 and ssp585)
³⁷⁸ than decrease ($n = 13$ for ssp126; $n = 12$ for ssp245 and ssp585) and the magnitude of increases
³⁷⁹ was greater than decreases for each GCM scenario. For decreases, the median percent difference
³⁸⁰ between average cover in 2018 and average cover in 2100 was -9% for ssp126, -18% for ssp245,
³⁸¹ and -24% for ssp585. For increases, the median percent difference between average cover in 2018
³⁸² and average cover in 2100 was 17% for ssp126, 34% for ssp245, and 79% for ssp585. The percent
³⁸³ differences show that projected increases in sagebrush cover are nearly twice the magnitude of
³⁸⁴ projected decreases for each GCM scenario, on average. Summing across core areas, 41711 -
³⁸⁵ 45474 km² of land is projected to experience increases in sagebrush cover on average, depending
³⁸⁶ on GCM scenario. 12978 - 16740 km² of land is projected to experience decreases in sagebrush
³⁸⁷ cover on average, depending on GCM scenario.

³⁸⁸ Figure 7 shows projections over time and space for the Salt Wells core area (as an example)
³⁸⁹ under the ssp585 climate forcing scenario. Spatial heterogeneity is maintained because of the

390 spatial offset included in the model, but heterogeneity is smoothed somewhat, resulting in slightly
391 lower spatial variance. Lower spatial variance can impact the calculation of the proportion of grid
392 cells with cover over or under the nesting and summer habitat targets. At this core area, projections
393 show sagebrush declining in most of the area with a hotspot of increasing sagebrush on the western
394 edge (Fig. 7).

395 Notable declines in sagebrush cover are projected for Bear River (BrRv), Elk Basin East
396 (ElBE), Jackson (Jcks), Little Mountain (LttM), and North Gillette (NrthGll) core areas (Fig. 6).
397 These same core areas may become suboptimal for sage-grouse over the long-term, as projections
398 suggest the proportion of cells in Bear River, Little Mountain, and Jackson that exceed the sage-
399 grouse nesting target drop below 50% at some point in the future (Figs. 8 and 9B). Twelve core
400 areas are projected to switch from suboptimal to optimal for sage-grouse by crossing the 50%
401 threshold in the future (Figs. 8 and 9D). The most common projection ($n = 16$) is for currently
402 suboptimal core areas to remain suboptimal, even though most will experience gains in sagebrush
403 cover (Fig. 9).

404 Most sage-grouse population growth rates have confidence intervals that overlap one, indicating
405 a stable population (Fig. 9). However, the mean growth rates suggest that 12 of the 16 core areas
406 projected to remain suboptimal already have declining sage-grouse populations (Fig. 9C). Ten of
407 the 12 core areas projected to switch from suboptimal to optimal have mean sage-grouse population
408 growth rates that are negative (Fig. 9D).

409 [Figure 6 about here.]

410 [Figure 7 about here.]

411 [Figure 8 about here.]

412 [Figure 9 about here.]

413 **Drivers of sensitivity classifications**

414 The best model for predicting precipitation sensitivity class (negative or positive) failed to beat a
415 null model of random classification. Therefore, we do not discuss results from the precipitation
416 sensitivity classification model. The best model for predicting temperature sensitivity class (neg-
417 ative or positive) included six non-zero covariates, all of which were soil properties (Table 4). The
418 model achieved a leave-one-out cross-validation accuracy score of 0.66 and an F1 score of 0.78
419 (F1 <= 0.5 indicates a poor model). The covariate with the largest LASSO-penalized coefficient
420 value was the average (averaged over grid cells and then over depths) of the 95th percentile of
421 sand percentage ($\hat{\beta} = 0.48$). All coefficient values were positive, meaning that increases in the
422 covariates values increased the odds that sensitivity to temperature will be positive.

423 [Table 4 about here.]

424 **Discussion**

425 Projections of sagebrush cover represent the combined effect of sensitivity to the climate drivers
426 and the magnitude of change expected in the climate driver in the future. We found that sagebrush
427 performance at most core areas showed positive sensitivity to temperature and negative sensitivity
428 to precipitation. Because average temperature is expected to increase in Wyoming in the future and
429 average precipitation is expected to remain relatively constant, we project an increase in sagebrush
430 cover at most core areas across Wyoming. Moreover, projected increases were larger in magnitude
431 than decreases and increases were projected on about four times larger land area (about 45,000 km²
432 expected to experience increases relative to about 13,000 km² expected to experience decreases,
433 on average). This finding suggests that few core areas are “lost causes” in terms of maintaining
434 existing sagebrush cover in the future. Continued conservation of these core areas has the potential
435 to increase sage-grouse populations in the future because the extent of the landscape with sagebrush
436 cover that exceeds the nesting threshold is expected to increase for several core areas (Fig. 8). Even
437 when the threshold is not projected to be exceeded, sagebrush cover is most commonly projected to

438 increase. While sagebrush is a key component of sage-grouse habitat, our models do not currently
439 consider other factors that can affect habitat quality, including herbaceous vegetation, structure and
440 configuration of sagebrush on the landscape, or disturbances (Fedy et al. 2014).

441 The most common climate response across the core areas was a positive effect of temperature
442 on sagebrush performance. This finding is consistent with theoretical and empirical research sug-
443 gesting that plants at the cold-limited edge of their distribution may benefit from global climate
444 change (Amburgey et al. 2018, Kleinhesselink and Adler 2018, Renwick et al. 2018). The finding
445 is also consistent with results across a broader range of the sagebrush distribution using these same
446 data sources (Rigge et al. 2021). Recent mechanistic modeling across the sagebrush biome also
447 suggests that increases in temperature will benefit sagebrush in high elevation portions of its range,
448 like Wyoming (Palmquist et al. 2021). Palmquist et al. (2021) showed that soil moisture will likely
449 remain adequate under a warming climate in warm, moisture-limited areas. Other studies have also
450 found positive effects of temperature increases at high elevation sagebrush sites, likely due to ear-
451 lier snowmelt and a longer growing season (Perfors et al. 2003, Harte et al. 2015). Our statistical
452 models appear to reflect these underlying mechanistic explanations at a majority of core areas. A
453 negative effect of increased precipitation combined with a positive effect of temperature could
454 reflect sagebrush responding negatively to late season snow in colder years and positively to earlier
455 snowmelt in warmer years.

456 Climate responses were not uniform across core areas, however. The models showed positive
457 and negative responses to both precipitation and temperature annual anomalies. Opposing effects
458 of weather on sagebrush performance are not uncommon (Renwick et al. 2018, Palmquist et al.
459 2021). Regional, landscape, and local gradients in average climate (Kleinhesselink and Adler
460 2018), soil conditions (Schlaepfer et al. 2012), and subspecies composition (Rosentreter 2005)
461 can have a strong influence on sagebrush responses to weather and climate. Our analysis of the
462 drivers of estimated sensitivities yielded little insight, though. The model for precipitation sensi-
463 tivity classification was no better than a random classifier. The model for temperature sensitivity
464 classification showed that several soil properties predict whether temperature sensitivity will be

positive or negative. Two covariates stood out with higher coefficient values: the average 95th percentail of sand percentage and the average 95th percentile of clay percentage. The odds of temperature sensitivity being positive (warmer temperatures → increase in sagebrush cover) increased with both of those covariates. Based on these results, it appears that sagebrush climate response is mediated by the extremes of soil properties within a landscape. Indeed, all non-zero coefficients were associated with either 5th percentile or 95th percentile statistics (Table 4). Thus, landscape level responses of sagebrush cover to climate may be mostly influenced by sagebrush that exist outside of average soil conditions.

The biggest limiation of our study is that we only quantified the direct effects of climate on sagebrush performance. The indirect effects of climate change and other non-climate related effects might be more influential. In particular, the fire-cheatgrass invasion cycle has been implicated as the major driver of sagebrush loss across most of its historical range. Recent modeling suggests that parts of Wyoming may become more suitable for cheatgrass but that cheatgrass invasion could be limited if disturbances that reduce native grass and shrub cover are limited (Palmquist et al. 2021). Hotter and drier conditions in the future will likely increase fire risk throughout Wyoming shrublands, meaning it could be difficult to limit cheatgrass invasion if fires become widespread. Nonetheless, our results corroborate those of Palmquist et al. (2021) by suggesting that climate change alone should benefit, or at least not significantly disadvantage, sagebush in Wyoming.

Our sagebrush projections can be used as part of a decision-support toolbox for managers in Wyoming. The projections are also useful for generating hypotheses and scientific questions. For example, what conditions lead to two core areas in the same region having divergent responses to temperature (North Gillette versus Thunder Basin, Fig. 4A)? Observational and experimental studies could help explain the divergent responses. Such explanations are critical to guide region-wide management of sagebrush landscapes in the face of climate change and potential cheatgrass invasion.

490 **Implications for sage-grouse management**

491 Sage-grouse are sagebrush-obligate species, meaning any increase in sagebrush cover likely bene-
492 fits sage-grouse but consideration of other habitat components also affect habitat quality for sage-
493 grouse (Fedy et al. 2014). Although not all core areas are projected to increase in sagebrush cover,
494 the magnitude of increase and the area over which we project increases far outweighs projected
495 declines. These results highlight the importance of active and adaptive management in Wyoming's
496 sage-grouse core areas, which contain about 37% of all sage-grouse (Fedy et al. 2014). Potential
497 management actions include reducing cheatgrass invasion to the greatest extent possible and lim-
498 iting disturbances in core areas. These management actions are important because our results, and
499 others, indicate that climate change per se is not going to cause declines in sagebrush in Wyoming.
500 In part, this is good news because managing disturbances and plant invasions is more feasible than
501 managing global climate change.

502 Even still, effectively conserving all of the core areas may not be enough. Sage-grouse use vast
503 areas outside of the core areas as well, particularly in the apex of the population cycles (Heinrichs
504 et al. 2019). Sage-grouse require diverse resource compositions across life stages, with an upper
505 limit of annual life-time home ranges estimated at ~2975 km² (Connelly et al. 2000b, Connelly
506 et al. 2000a). Maintaining large intact landscapes inside and outside of core areas (Heinrichs
507 et al. 2019) will be necessary to ensure viable sage-grouse populations persist. Our models help
508 to identify sagebrush habitats that persist into the future given climate change, which should be
509 protected from disturbances. Areas with projected sagebrush declines may need to be more closely
510 managed.

511 **Acknowledgements**

512 This study was funded by the Bureau of Land Management and the US Geological Survey. Any use
513 of trade, firm, or product names is for descriptive purposes only and does not imply endorsement by
514 the U.S. government. We thank Darren Long for reviewing preliminary versions of the manuscript.

515 **References**

- 516 Amburgey, S. M., D. A. W. Miller, E. H. C. Grant, T. A. G. Rittenhouse, M. F. Benard, J. L.
517 Richardson, M. C. Urban, W. Hughson, A. B. Brand, C. J. Davis, C. R. Hardin, P. W. C.
518 Paton, C. J. Raithel, R. A. Relyea, A. F. Scott, D. K. Skelly, D. E. Skidds, C. K. Smith, and E.
519 E. Werner. 2018. Range position and climate sensitivity: The structure of among-population
520 demographic responses to climatic variation. *Global Change Biology* 24:439–454.
- 521 Balch, J. K., B. A. Bradley, C. M. D'Antonio, and J. Gómez-Dans. 2013. Introduced annual
522 grass increases regional fire activity across the arid western USA (1980–2009). *Global
523 Change Biology* 19:173–183.
- 524 Boettiger, C., M. Bode, J. N. Sanchirico, J. LaRiviere, A. Hastings, and P. R. Armsworth.
525 2016. Optimal management of a stochastically varying population when policy adjustment
526 is costly. *Ecological Applications* 26:808–817.
- 527 Bradley, B. A. 2009. Regional analysis of the impacts of climate change on cheatgrass invasion
528 shows potential risk and opportunity. *Global Change Biology* 15:196–208.
- 529 Cardinale, B. J., J. E. Duffy, A. Gonzalez, D. U. Hooper, C. Perrings, P. Venail, A. Narwani,
530 G. M. Mace, D. Tilman, D. A. Wardle, A. P. Kinzig, G. C. Daily, M. Loreau, J. B. Grace,
531 A. Larigauderie, D. S. Srivastava, and S. Naeem. 2012. Biodiversity loss and its impact on
532 humanity. *Nature* 486:59–67.
- 533 Carlisle, J., and A. Chalfoun. 2020. The abundance of Greater Sage-Grouse as a proxy for the
534 abundance of sagebrush-associated songbirds in Wyoming, USA. *Avian Conservation and
535 Ecology* 15.
- 536 Chambers, J. C., B. A. Roundy, R. R. Blank, S. E. Meyer, and A. Whittaker. 2007. What
537 Makes Great Basin Sagebrush Ecosystems Invasive by *Bromus Tectorum*? *Ecological
538 Monographs* 77:117–145.

- 539 Chaney, N. W., B. Minasny, J. D. Herman, T. W. Nauman, C. W. Brungard, C. L. S. Morgan,
540 A. B. McBratney, E. F. Wood, and Y. Yimam. 2019. POLARIS Soil Properties: 30-m
541 Probabilistic Maps of Soil Properties Over the Contiguous United States. *Water Resources*
542 Research 55:2916–2938.
- 543 Clark, J. S., S. R. Carpenter, M. Barber, S. Collins, A. Dobson, J. A. Foley, D. M. Lodge, M.
544 Pascual, R. Pielke, W. Pizer, C. Pringle, W. V. Reid, K. A. Rose, O. Sala, W. H. Schlesinger,
545 D. H. Wall, and D. Wear. 2001. Ecological Forecasts: An Emerging Imperative. *Science*
546 293:657–660.
- 547 Conn, P. B., D. S. Johnson, J. M. V. Hoef, M. B. Hooten, J. M. London, and P. L. Boveng. 2015.
548 Using spatiotemporal statistical models to estimate animal abundance and infer ecological
549 dynamics from survey counts. *Ecological Monographs* 85:235–252.
- 550 Conn, P. B., D. S. Johnson, P. J. Williams, S. R. Melin, and M. B. Hooten. 2018. A guide to
551 Bayesian model checking for ecologists. *Ecological Monographs* 88:526–542.
- 552 Connelly, J. W., S. T. Knick, M. A. Schroeder, and S. J. Stiver. 2000a. Conservation assess-
553 ment of greater sage-grouse and sagebrush habitats. Western Association of Fish; Wildlife
554 Agencies, Cheyenne, Wyoming.
- 555 Connelly, J. W., K. P. Reese, R. A. Fischer, and W. L. Wakkinen. 2000b. Response of a Sage
556 Grouse Breeding Population to Fire in Southeastern Idaho. *Wildlife Society Bulletin (1973-
557 2006)* 28:90–96.
- 558 Dietze, M. C., A. Fox, L. M. Beck-Johnson, J. L. Betancourt, M. B. Hooten, C. S. Jarnevich,
559 T. H. Keitt, M. A. Kenney, C. M. Laney, L. G. Larsen, H. W. Loescher, C. K. Lunch, B.
560 C. Pijanowski, J. T. Randerson, E. K. Read, A. T. Tredennick, R. Vargas, K. C. Weathers,
561 and E. P. White. 2018. Iterative near-term ecological forecasting: Needs, opportunities, and
562 challenges. *Proceedings of the National Academy of Sciences* 115:1424–1432.

- 563 Edmunds, D. R., C. L. Aldridge, M. S. O'Donnell, and A. P. Monroe. 2018. Greater sage-grouse
564 population trends across Wyoming. *The Journal of Wildlife Management* 82:397–412.
- 565 Eyring, V., S. Bony, G. A. Meehl, C. A. Senior, B. Stevens, R. J. Stouffer, and K. E. Taylor.
566 2016. Overview of the Coupled Model Intercomparison Project Phase 6 (CMIP6) experi-
567 mental design and organization. *Geoscientific Model Development* 9:1937–1958.
- 568 Farber, S., R. Costanza, D. L. Childers, J. Erickson, K. Gross, M. Grove, C. S. Hopkinson, J.
569 Kahn, S. Pincetl, A. Troy, P. Warren, and M. Wilson. 2006. Linking Ecology and Economics
570 for Ecosystem Management. *BioScience* 56:121–133.
- 571 Fedy, B. C., K. E. Doherty, C. L. Aldridge, M. O'Donnell, J. L. Beck, B. Bedrosian, D. Gummer,
572 M. J. Holloran, G. D. Johnson, N. W. Kaczor, C. P. Kirol, C. A. Mandich, D. Marshall, G.
573 McKee, C. Olson, A. C. Pratt, C. C. Swanson, and B. L. Walker. 2014. Habitat prioritization
574 across large landscapes, multiple seasons, and novel areas: An example using greater sage-
575 grouse in Wyoming. *Wildlife Monographs* 190:1–39.
- 576 Gelman, A., and J. Hill. 2006. Data Analysis Using Regression and Multilevel/Hierarchical
577 Models. Cambridge University Press.
- 578 Gelman, A., and D. B. Rubin. 1992. Inference from Iterative Simulation Using Multiple Se-
579 quences. *Statistical Science* 7:457–472.
- 580 Guo, J., J. Gabry, B. Goodrich, S. Weber, D. Lee, K. Sakrejda, M. Martin, T. of C. University, O.
581 Sklyar (R/cxxfunplus.R), T. R. C. Team (R/pairs.R, R/dynGet.R), J. Oehlschlaegel-Akiyoshi
582 (R/pairs.R), J. Maddock (gamma.hpp), P. Bristow (gamma.hpp), N. Agrawal (gamma.hpp),
583 C. Kormanyos (gamma.hpp), and B. Steve. 2020, July. Rstan: R Interface to Stan.
- 584 Harte, J., S. R. Saleska, and C. Levy. 2015. Convergent ecosystem responses to 23-year ambient
585 and manipulated warming link advancing snowmelt and shrub encroachment to transient and
586 long-term climate–soil carbon feedback. *Global Change Biology* 21:2349–2356.

- 587 Heinrichs, J. A., M. S. O'Donnell, C. L. Aldridge, S. L. Garman, and C. G. Homer. 2019.
588 Influences of potential oil and gas development and future climate on Sage-grouse declines
589 and redistribution. *Ecological Applications* 29:e01912.
- 590 Hobbs, N. T., and M. B. Hooten. 2015. *Bayesian Models: A Statistical Primer for Ecologists*.
591 Princeton University Press.
- 592 Ives, A. R., B. Dennis, K. L. Cottingham, and S. R. Carpenter. 2003. Estimating Commu-
593 nity Stability and Ecological Interactions from Time-Series Data. *Ecological Monographs*
594 73:301–330.
- 595 Jia, H., and A. Chong. 2020. *Epwshiftr: Create Future 'EnergyPlus' Weather Files using*
596 *'CMIP6' Data.*
- 597 Kleinhesselink, A. R., and P. B. Adler. 2018. The response of big sagebrush (*Artemisia triden-*
598 *tata*) to interannual climate variation changes across its range. *Ecology* 99:1139–1149.
- 599 McDonald, T., A. M. (HIP. sampling methods), M. Kleinsausser, and S. E. (Auto. testing and
600 Travis). 2020, July. *SDraw: Spatially Balanced Samples of Spatial Objects*.
- 601 McShane, T. O., P. D. Hirsch, T. C. Trung, A. N. Songorwa, A. Kinzig, B. Monteferri, D.
602 Mutekanga, H. V. Thang, J. L. Dammert, M. Pulgar-Vidal, M. Welch-Devine, J. Peter Bro-
603 sius, P. Coppolillo, and S. O'Connor. 2011. Hard choices: Making trade-offs between
604 biodiversity conservation and human well-being. *Biological Conservation* 144:966–972.
- 605 Nepstad, D. C., C. M. Stickler, B. S.-. Filho, and F. Merry. 2008. Interactions among Amazon
606 land use, forests and climate: Prospects for a near-term forest tipping point. *Philosophical*
607 *Transactions of the Royal Society B: Biological Sciences* 363:1737–1746.
- 608 Ogle, K., and J. J. Barber. 2020. Ensuring identifiability in hierarchical mixed effects Bayesian
609 models. *Ecological Applications* 30:e02159.

- 610 Palmquist, K. A., D. R. Schlaepfer, R. R. Renne, S. C. Torbit, K. E. Doherty, T. E. Remington,
611 G. Watson, J. B. Bradford, and W. K. Lauenroth. 2021. Divergent climate change effects
612 on widespread dryland plant communities driven by climatic and ecohydrological gradients.
613 Global Change Biology n/a.
- 614 Pastick, N. J., B. K. Wylie, M. B. Rigge, D. Dahal, S. P. Boyte, M. O. Jones, B. W. Allred,
615 S. Parajuli, and Z. Wu. 2021. Rapid Monitoring of the Abundance and Spread of Exotic
616 Annual Grasses in the Western United States Using Remote Sensing and Machine Learning.
617 AGU Advances 2:e2020AV000298.
- 618 Pedregosa, F., G. Varoquaux, A. Gramfort, V. Michel, B. Thirion, O. Grisel, M. Blondel, P.
619 Prettenhofer, R. Weiss, V. Dubourg, J. Vanderplas, A. Passos, D. Cournapeau, M. Brucher,
620 M. Perrot, and É. Duchesnay. 2011. Scikit-learn: Machine Learning in Python. Journal of
621 Machine Learning Research 12:2825–2830.
- 622 Perfors, T., J. Harte, and S. E. Alter. 2003. Enhanced growth of sagebrush (*Artemisia tridentata*)
623 in response to manipulated ecosystem warming. Global Change Biology 9:736–742.
- 624 Pilliod, D. S., M. I. Jeffries, R. S. Arkle, and D. H. Olson. 2020. Reptiles Under the Conser-
625 vation Umbrella of the Greater Sage-Grouse. The Journal of Wildlife Management 84:478–
626 491.
- 627 Powers, R. P., and W. Jetz. 2019. Global habitat loss and extinction risk of terrestrial vertebrates
628 under future land-use-change scenarios. Nature Climate Change 9:323–329.
- 629 R Core Team. 2020. R: A Language and Environment for Statistical Computing. R Foundation
630 for Statistical Computing.
- 631 Renwick, K. M., C. Curtis, A. R. Kleinhesselink, D. Schlaepfer, B. A. Bradley, C. L. Aldridge,
632 B. Poulter, and P. B. Adler. 2018. Multi-model comparison highlights consistency in pre-
633 dicted effect of warming on a semi-arid shrub. Global Change Biology 24:424–438.

- 634 Rigge, M., C. Homer, L. Cleeves, D. K. Meyer, B. Bunde, H. Shi, G. Xian, S. Schell, and M.
635 Bobo. 2020. Quantifying Western U.S. Rangelands as Fractional Components with Multi-
636 Resolution Remote Sensing and In Situ Data. *Remote Sensing* 12:412.
- 637 Rigge, M., H. Shi, and K. Postma. 2021. Projected change in rangeland fractional compo-
638 nent cover across the sagebrush biome under climate change through 2085. *Ecosphere*
639 12:e03538.
- 640 Rosentreter, R. 2005. Sagebrush identification, ecology, and palatability relative to sage-grouse.
641 In: Shaw, Nancy L.; Pellatt, Mike; Monsen, Stephen B., comps. 2005. Sage-grouse habitat
642 restoration symposium proceedings; 2001 June 4-7, Boise, ID. Proc. RMRS-P-38. Fort
643 Collins, CO: U.S. Department of Agriculture, Forest Service, Rocky Mountain Research
644 Station. p. 3-16 038.
- 645 Rowland, M. M., M. J. Wisdom, L. H. Suring, and C. W. Meinke. 2006. Greater sage-
646 grouse as an umbrella species for sagebrush-associated vertebrates. *Biological Conservation*
647 129:323–335.
- 648 Rupp, D. E., J. T. Abatzoglou, K. C. Hegewisch, and P. W. Mote. 2013. Evaluation of CMIP5
649 20th century climate simulations for the Pacific Northwest USA. *Journal of Geophysical
650 Research: Atmospheres* 118:10, 884–10, 906.
- 651 Sala, O. E., F. S. Chapin, III, J. J. Armesto, E. Berlow, J. Bloomfield, R. Dirzo, E. Huber-
652 Sanwald, L. F. Huenneke, R. B. Jackson, A. Kinzig, R. Leemans, D. M. Lodge, H. A.
653 Mooney, M. Oesterheld, N. L. Poff, M. T. Sykes, B. H. Walker, M. Walker, and D. H. Wall.
654 2000. Global Biodiversity Scenarios for the Year 2100. *Science* 287:1770–1774.
- 655 Schlaepfer, D. R., W. K. Lauenroth, and J. B. Bradford. 2012. Ecohydrological niche of sage-
656 brush ecosystems. *Ecohydrology* 5:453–466.
- 657 Smith, I. T., J. L. Rachlow, L. K. Svancara, L. A. McMahon, and S. J. Knetter. 2019. Habitat
658 specialists as conservation umbrellas: Do areas managed for greater sage-grouse also protect

- 659 pygmy rabbits? *Ecosphere* 10:e02827.
- 660 Stan Development Team. 2020. Stan Modeling Language Users Guide and Reference Manual,
- 661 2.12.2.
- 662 Stiver, S. J., E. T. Rinkes, D. E. Naugle, P. D. Makela, D. A. Nance, and J. W. Karl. 2015.
- 663 Sage-grouse Habitat Assessment Framework: A Multiscale Assessment Tool. Technical
- 664 Reference 6710-1. Bureau of Land Management; Western Association of Fish; Wildlife
- 665 Agencies, Denver, Colorado.
- 666 Tredennick, A. T., M. B. Hooten, C. L. Aldridge, C. G. Homer, A. R. Kleinhesselink, and P.
- 667 B. Adler. 2016. Forecasting climate change impacts on plant populations over large spatial
- 668 extents. *Ecosphere* 7:e01525.
- 669 Van Rossum, G., and F. L. Drake. 2009. Python 3 Reference Manual. CreateSpace, Scotts
- 670 Valley, CA.
- 671 Walters, C. J., and R. Hilborn. 1978. Ecological Optimization and Adaptive Management.
- 672 Annual Review of Ecology and Systematics 9:157–188.

673

List of Figures

674	1	Observed time series of percent cover for each core area from the Back-In-Time product. Line shows mean cover in each year across all cells (pixels). The shaded region shows the mean plus/minus the standard deviation across all cells (pixels) in each year. Note that the y-axis changes across panels.	32
675	2	(A) Relative errors of global circulation models when comparing historical projections to observed PRISM climate data within Wyoming sage-grouse core areas for the period 1985-2018. Values in the top panel (Combined) were subtracted from 1 and normalized for use as model weights when projecting sagebrush dynamics. GCMs are ordered from lowest (left) to highest (right) combined error. (B) Climate change projections for Greater South Pass (north) from all GCMs (light lines) and the weighted average of climate projections, which are proportional to the relative errors in panel A.	33
676	3	Posterior distributions of equilibrium cover calculated from fitted model parameters. The vertical black lines show the observed mean cover for each core area from 1985-2018.	34
677	4	Sensitivity of sagebrush cover to temperature and precipitation. Maps show the mean of the posterior distribution of sensitivity to temperature (A) and precipitation (B) for each core area. Panels to the right of the maps show the mean (crosshairs), 95% Bayesian credible interval (bold lines), and range of the posterior distributions (whiskers) of sensitivity to temperature (C) and precipitation (D) for each core area. Colors indicate positive (greens), negative (browns), and negligible (light grey) sensitivity. Sensitivity is defined as the log change in cover relative to equilibrium cover when a +1 standard deviation perturbation is applied to the climate effect in the fitted model for each core area.	35
678	5	Sensitivity of each core area to temperature and precipitation grouped by positive and negative responses to each climate driver. (A) Core areas with negative sensitivity to precipitation and positive sensitivity to temperature. (B) Core areas with positive sensitivity to precipitation and temperature, (C) Core areas with a negative sensitivity to precipitation and temperature. (D) Core areas with a positive sensitivity to precipitation and a negative sensitivity to temperature. Points show the posterior means and whiskers show the 95% Bayesian credible intervals. Dashed tan lines show where sensitivity equals zero. The panel labels also indicate the number of core areas (n) in each sensitivity quadrant.	36
679	6	Projections of sagebrush percent cover from 2018 to 2080 under three climate change scenarios (ssp indicated by colors) for each core area. The solid line is the median of the posterior predictive distribution; light shaded ribbon bounds the 68% BCI; very light shaded ribbon bounds the 95% BCI. Box and whiskers show the 68% (boxes) and 95% (whiskers) BCIs at discrete time horizons of 2020, 2040, 2060, and 2080. The y-axis scale differs across plots.	37

713	7	Projections of sagebrush percent cover (color bars indicate percent cover value) over space and time for the Salt Wells (SlW) core area. Projections are plotted from a single ensemble member (one parameter set) and using the ssp585 climate forcing scenario.	38
714			
715			
716			
717	8	Projections of the proportion of 100-meter cells within a core area where sagebrush percent cover exceeds the sage-grouse nesting threshold defined for each core area. The solid line is the median of the posterior predictive distribution; light shaded ribbon bounds the 68% BCI; very light shaded ribbon bounds the 95% BCI. The dashed horizontal line shows where the proportion of cells is equal to 50% of the area. The y-axis scale differs across plots.	39
718			
719			
720			
721			
722			
723	9	Sage-grouse population growth rates from Edmunds et al. (2018) for each core area, grouped by whether (A) the core area is currently more suitable and projected to remain more suitable, (B) currently more suitable and projected to become less suitable, (C) currently less suitable and projected to remain less suitable, and (D) currently less suitable and projected to become more suitable. ‘More suitable’ is defined as over 50% of cells with cover over the nesting threshold. ‘Less suitable’ is defined as fewer than 50% of cells with cover over the nesting threshold.	40
724			
725			
726			
727			
728			
729			

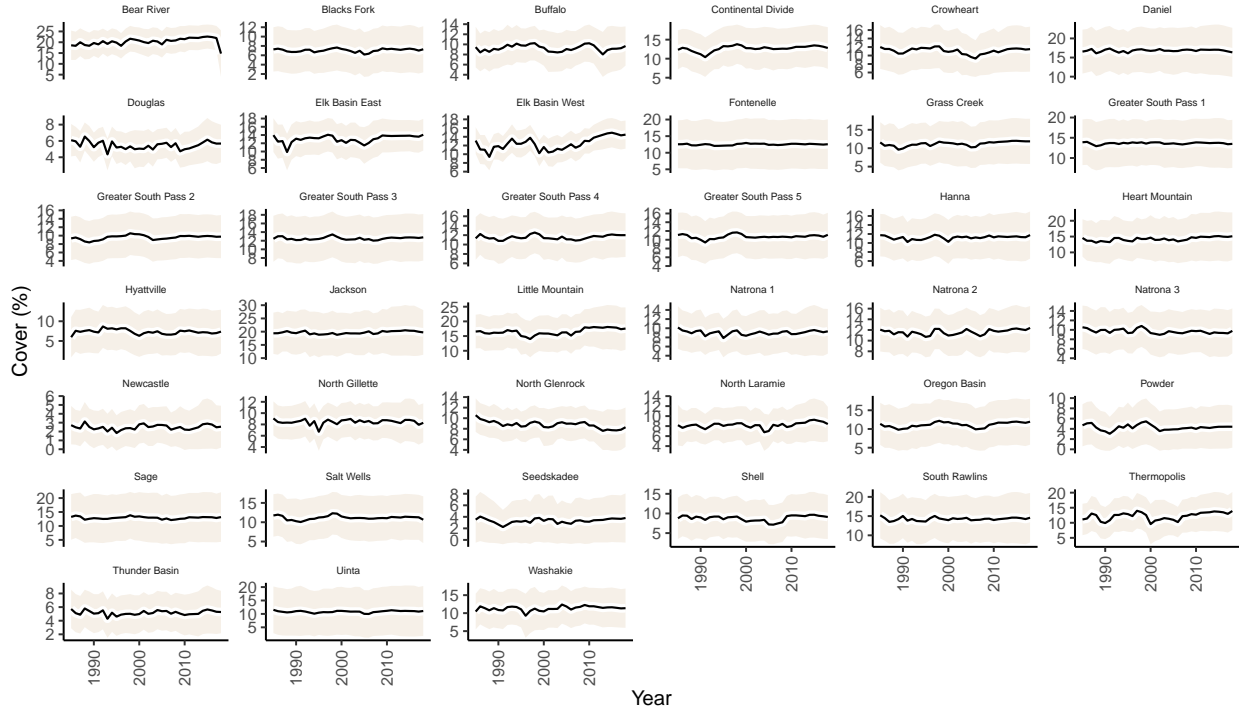


Figure 1: Observed time series of percent cover for each core area from the Back-In-Time product. Line shows mean cover in each year across all cells (pixels). The shaded region shows the mean plus/minus the standard deviation across all cells (pixels) in each year. Note that the y-axis changes across panels.

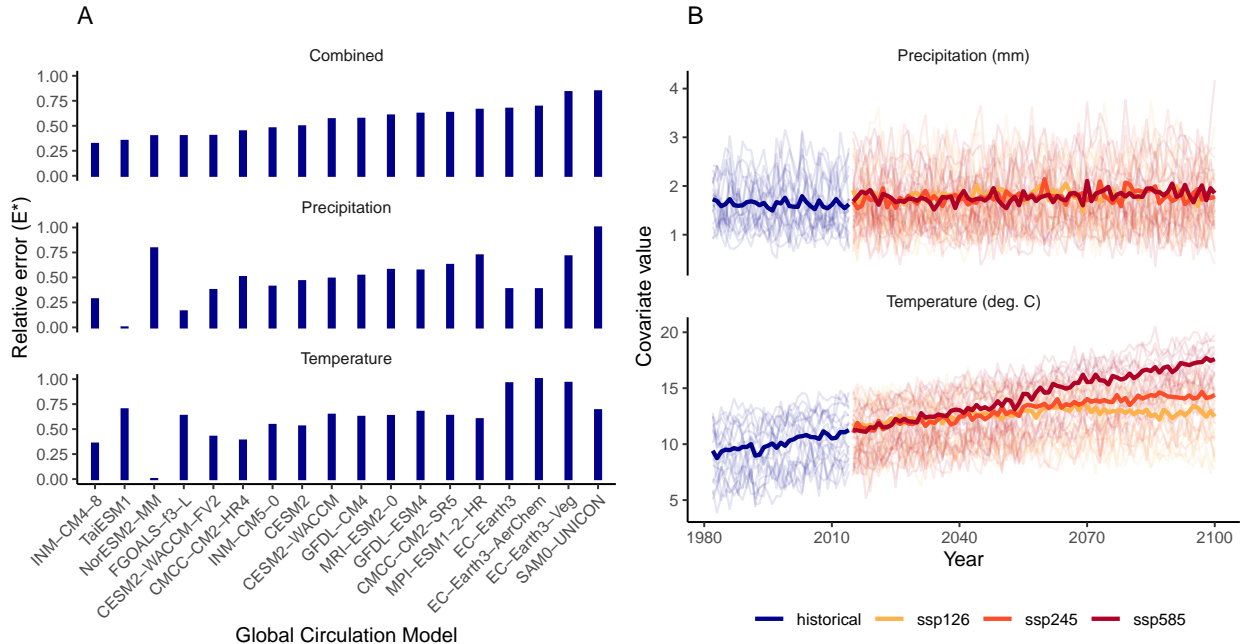


Figure 2: (A) Relative errors of global circulation models when comparing historical projections to observed PRISM climate data within Wyoming sage-grouse core areas for the period 1985–2018. Values in the top panel (Combined) were subtracted from 1 and normalized for use as model weights when projecting sagebrush dynamics. GCMs are ordered from lowest (left) to highest (right) combined error. (B) Climate change projections for Greater South Pass (north) from all GCMs (light lines) and the weighted average of climate projections, which are proportional to the relative errors in panel A.

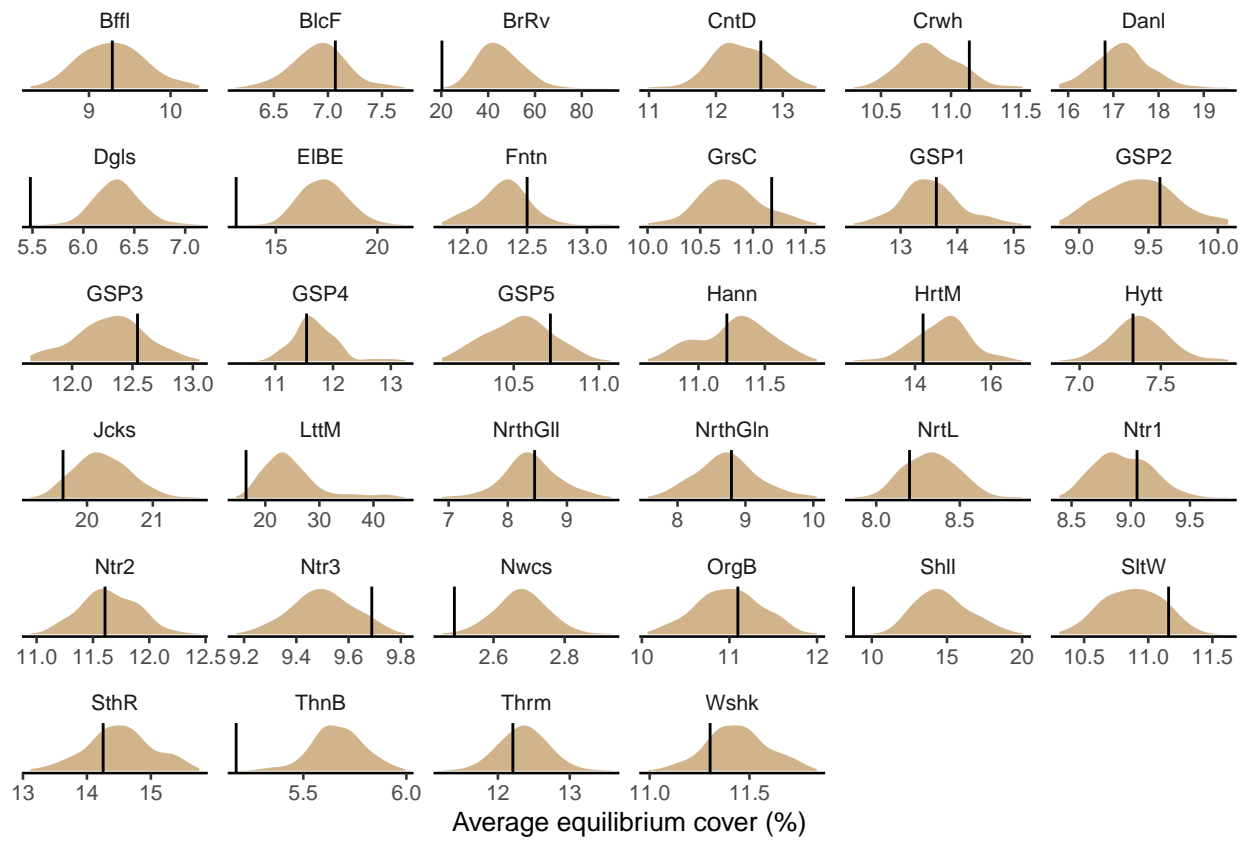


Figure 3: Posterior distributions of equilibrium cover calculated from fitted model parameters. The vertical black lines show the observed mean cover for each core area from 1985-2018.

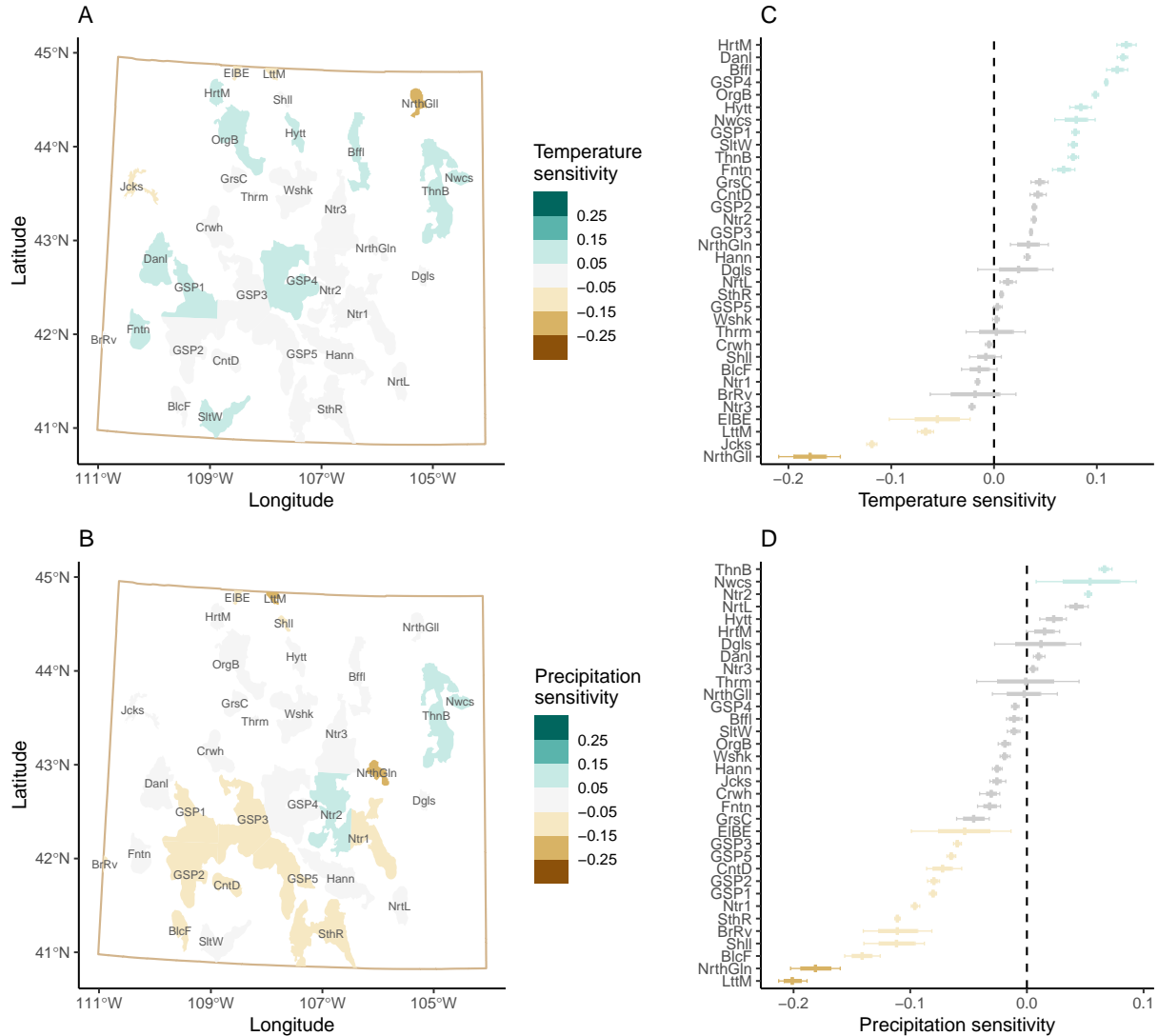


Figure 4: Sensitivity of sagebrush cover to temperature and precipitation. Maps show the mean of the posterior distribution of sensitivity to temperature (A) and precipitation (B) for each core area. Panels to the right of the maps show the mean (crosshairs), 95% Bayesian credible interval (bold lines), and range of the posterior distributions (whiskers) of sensitivity to temperature (C) and precipitation (D) for each core area. Colors indicate positive (greens), negative (browns), and negligible (light grey) sensitivity. Sensitivity is defined as the log change in cover relative to equilibrium cover when a +1 standard deviation perturbation is applied to the climate effect in the fitted model for each core area.

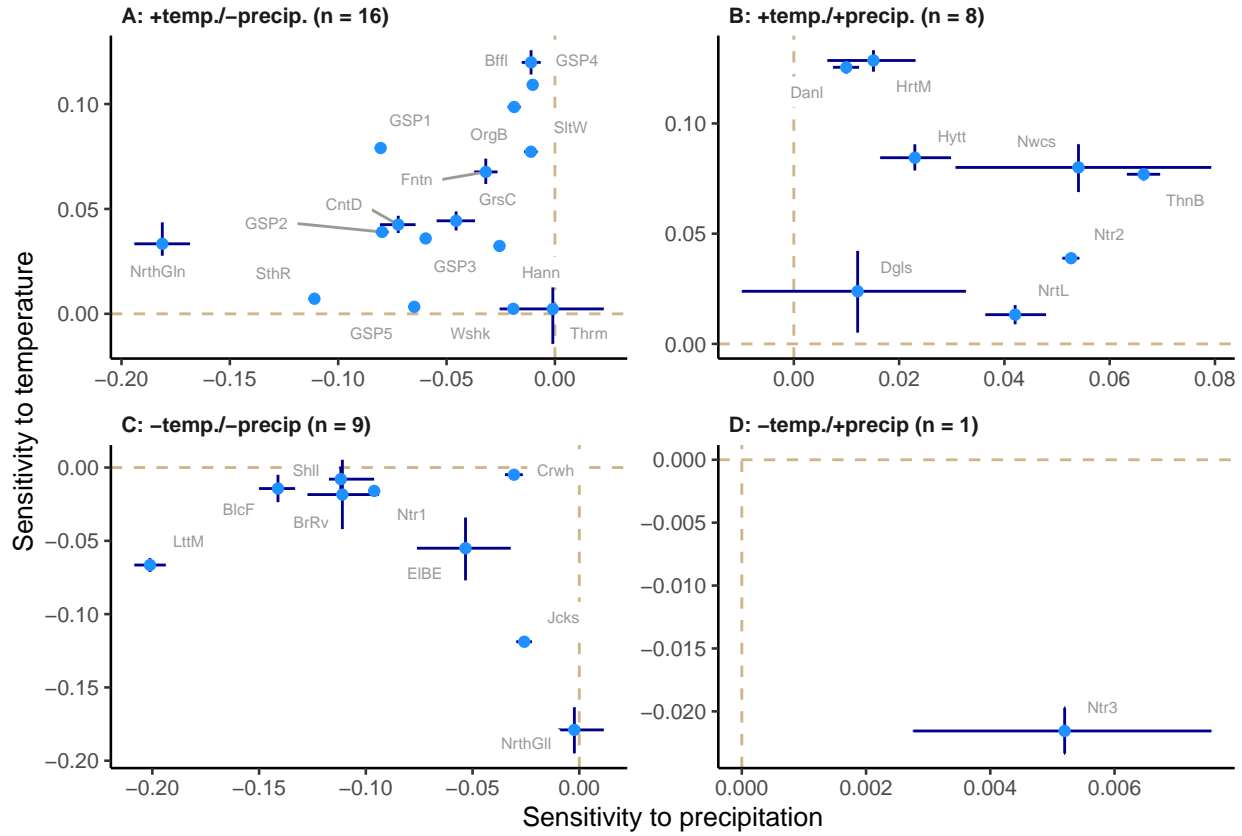


Figure 5: Sensitivity of each core area to temperature and precipitation grouped by positive and negative responses to each climate driver. (A) Core areas with negative sensitivity to precipitation and positive sensitivity to temperature. (B) Core areas with positive sensitivity to precipitation and temperature. (C) Core areas with a negative sensitivity to precipitation and temperature. (D) Core areas with a positive sensitivity to precipitation and a negative sensitivity to temperature. Points show the posterior means and whiskers show the 95% Bayesian credible intervals. Dashed tan lines show where sensitivity equals zero. The panel labels also indicate the number of core areas (n) in each sensitivity quadrant.

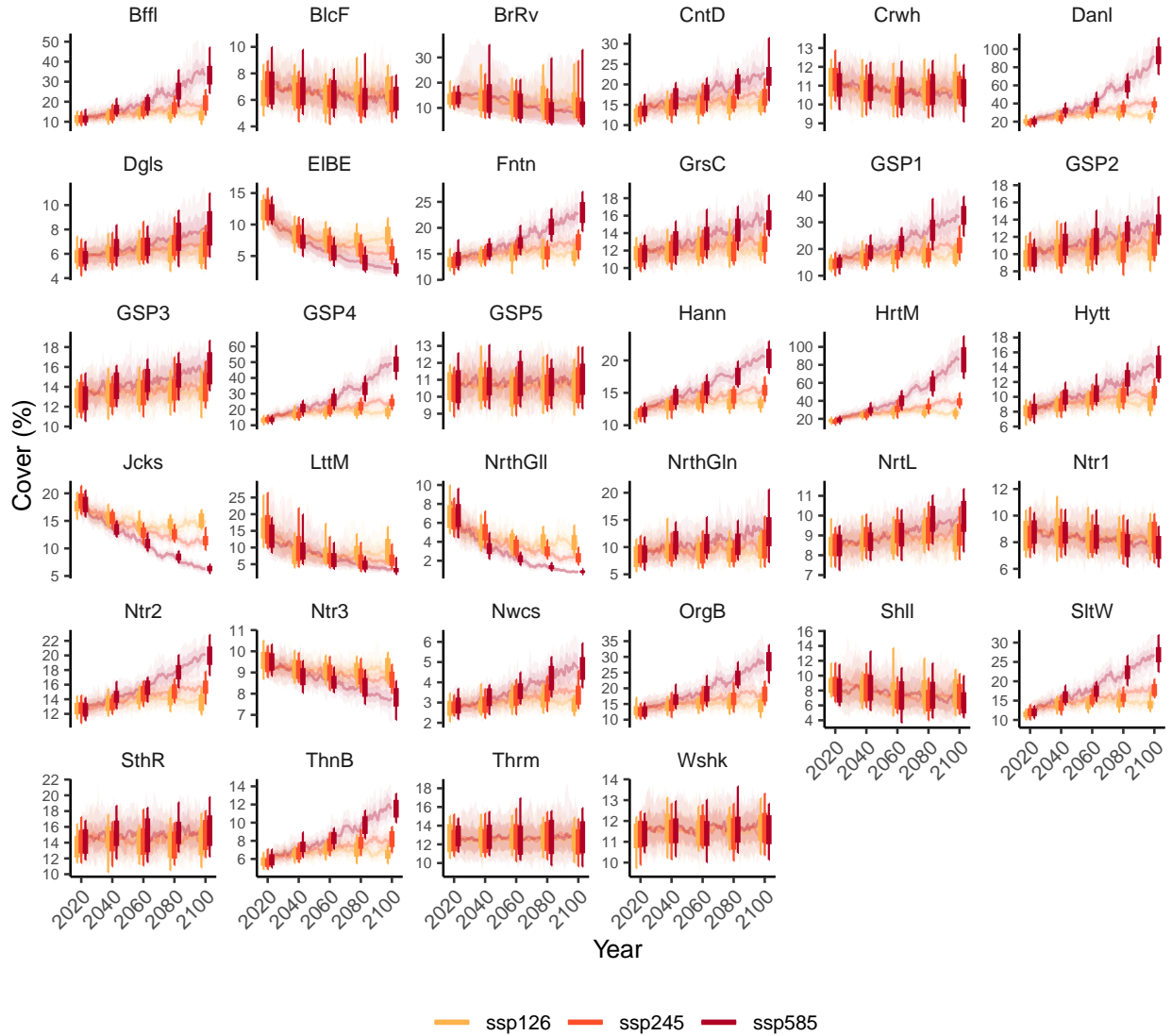


Figure 6: Projections of sagebrush percent cover from 2018 to 2080 under three climate change scenarios (ssp indicated by colors) for each core area. The solid line is the median of the posterior predictive distribution; light shaded ribbon bounds the 68% BCI; very light shaded ribbon bounds the 95% BCI. Box and whiskers show the 68% (boxes) and 95% (whiskers) BCIs at discrete time horizons of 2020, 2040, 2060, and 2080. The y-axis scale differs across plots.

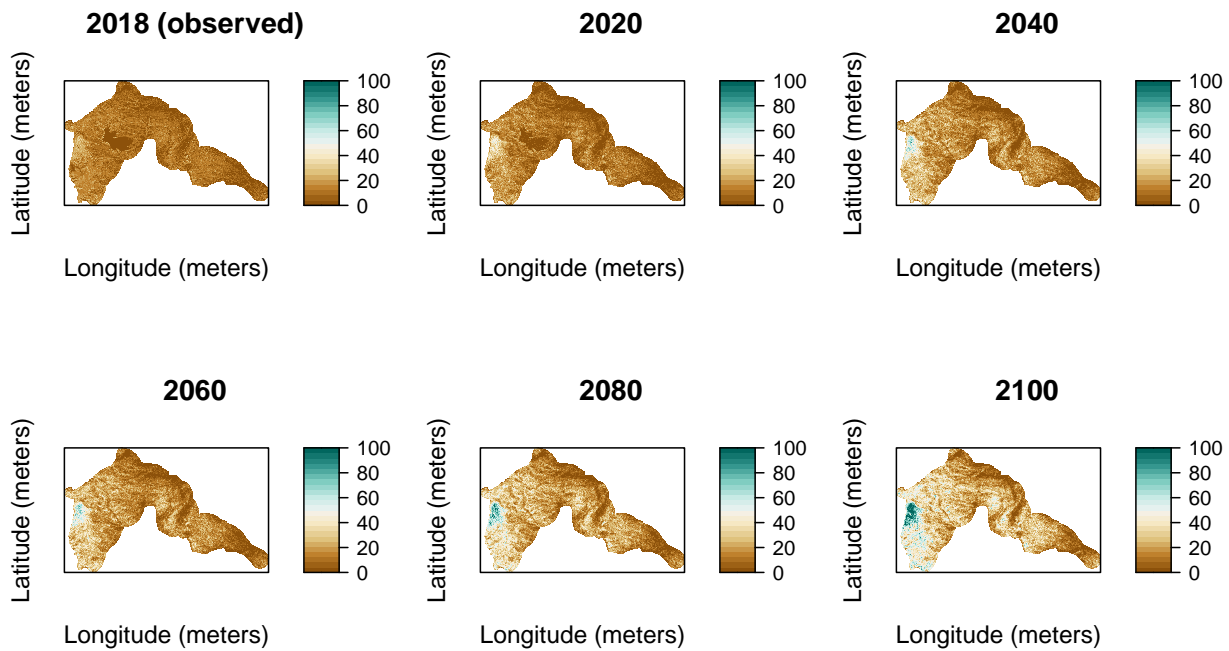


Figure 7: Projections of sagebrush percent cover (color bars indicate percent cover value) over space and time for the Salt Wells (SltW) core area. Projections are plotted from a single ensemble member (one parameter set) and using the ssp585 climate forcing scenario.

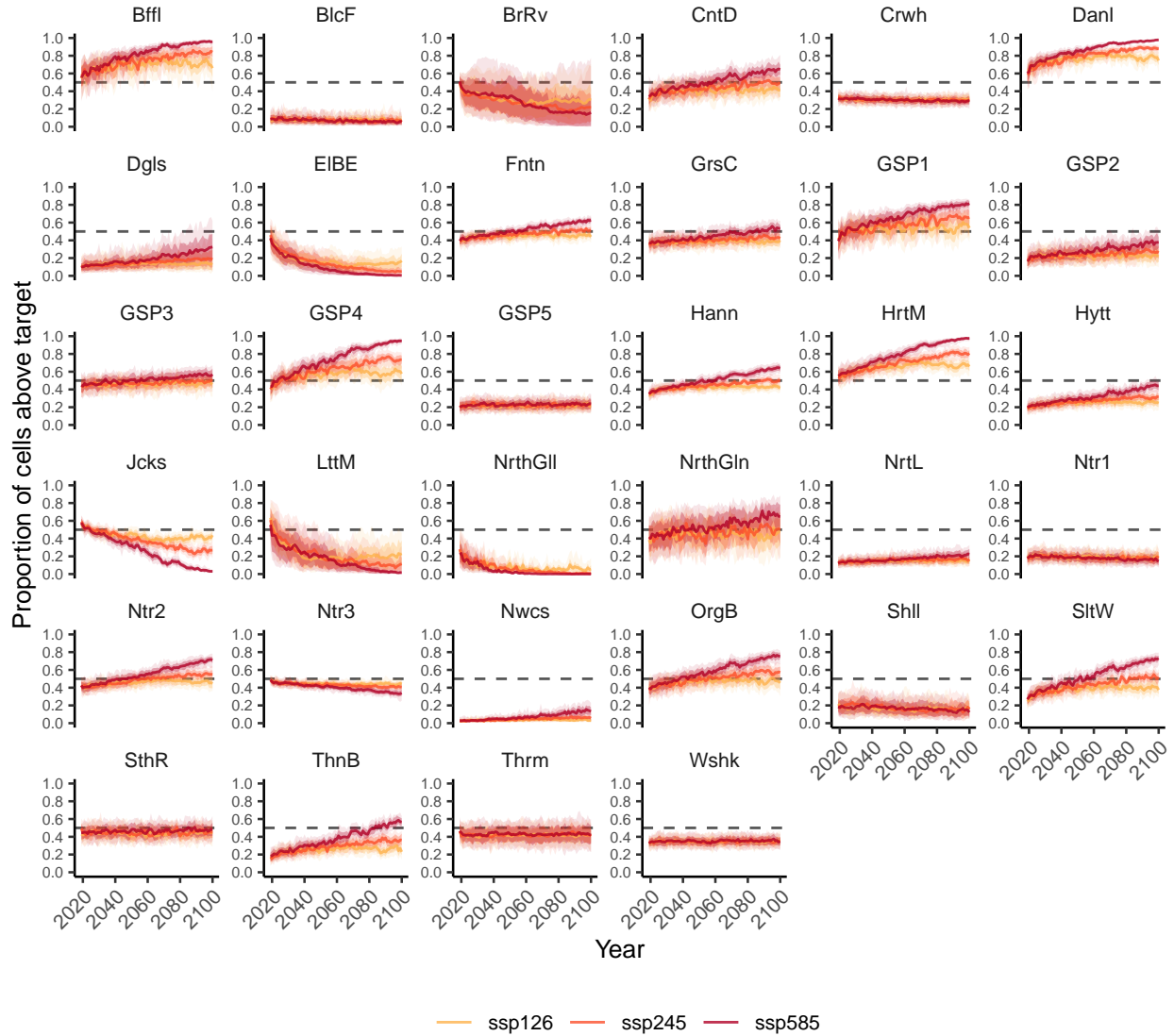


Figure 8: Projections of the proportion of 100-meter cells within a core area where sagebrush percent cover exceeds the sage-grouse nesting threshold defined for each core area. The solid line is the median of the posterior predictive distribution; light shaded ribbon bounds the 68% BCI; very light shaded ribbon bounds the 95% BCI. The dashed horizontal line shows where the proportion of cells is equal to 50% of the area. The y-axis scale differs across plots.

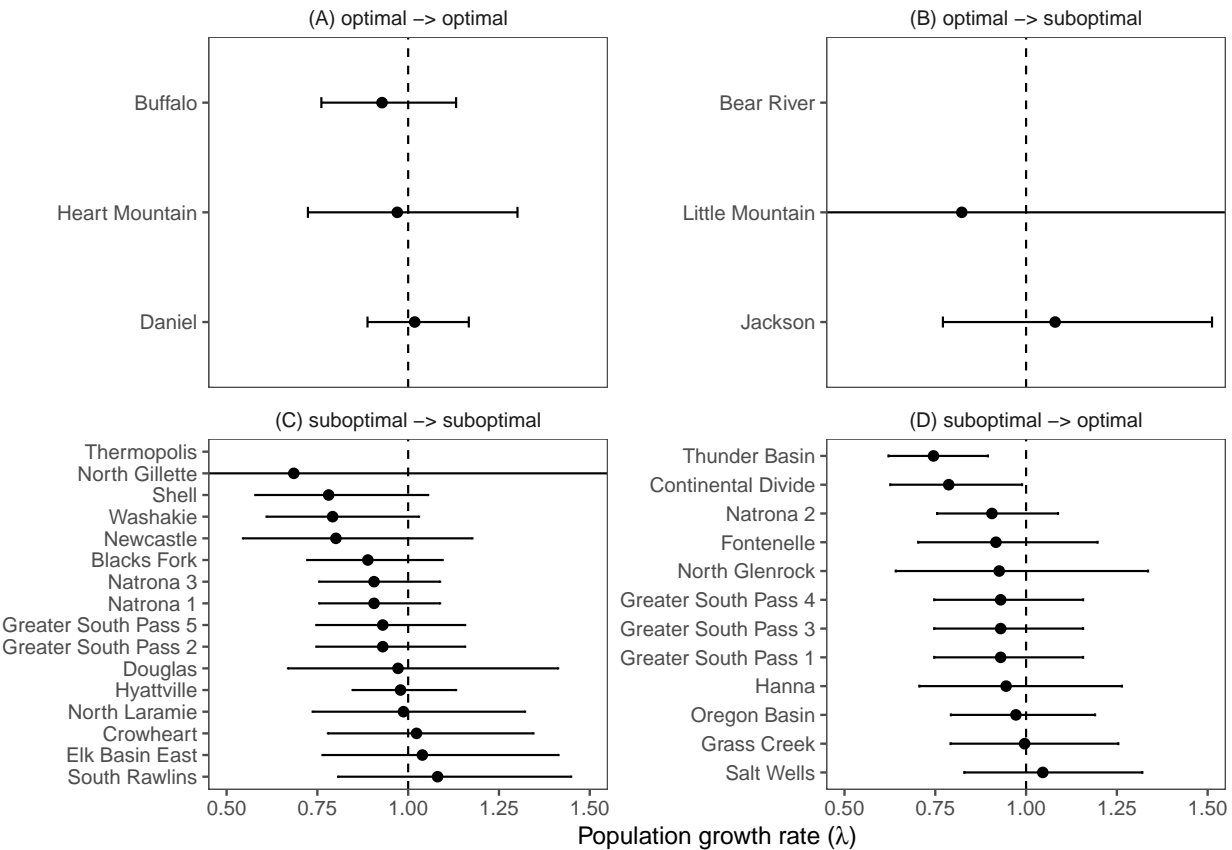


Figure 9: Sage-grouse population growth rates from Edmunds et al. (2018) for each core area, grouped by whether (A) the core area is currently more suitable and projected to remain more suitable, (B) currently more suitable and projected to become less suitable, (C) currently less suitable and projected to remain less suitable, and (D) currently less suitable and projected to become more suitable. ‘More suitable’ is defined as over 50% of cells with cover over the nesting threshold. ‘Less suitable’ is defined as fewer than 50% of cells with cover over the nesting threshold.

730 **List of Tables**

731 1	Prior distributions for the dynamic-additive spatiotemporal regression model of sagebrush cover.	42
733 2	Averages and variances of climate covariates over different time periods. Averages are average values over the core areas. Core area values were the weighted averages according to GCM weights. Variances are average variances over the core areas. Core area variances were computed over the weighted averages of values for each core area.	43
738 3	Results from colonization model for each core area. $\text{Pr}(\text{colonize} \mid \text{cover} = 0)$ reads, 'the probability of colonization given that current cover is zero.'	44
740 4	LASSO-penalized coefficient values for the selected model for classifying temperature sensitivity. Note that all predictor values were averaged over grid cells within a core area and then averaged over depth from surface. The 'alpha' covariate is: 'scale parameter inversely proportional to mean pore diameter'. Standard errors, confidence intervals, and/or p-values are not reported because these metrics are not yet available for penalized regression under frequentist framework.	45

Table 1: Prior distributions for the dynamic-additive spatiotemporal regression model of sagebrush cover.

Parameter	Definition	Distribution	Source
β_1	intercept	Normal(0.73, 1)	Tredennick et al. (2016)
β_2	density-dependence	Normal(0.72, 1)	Tredennick et al. (2016)
$\beta_{3\&4}$	effects of precipitation (β_3) and temperature (β_4)	Normal(0, 5)	–
γ	temporal random effects	Normal(0, σ_γ)	–
σ_γ	standard deviation of temporal random effects	Cauchy(0, 2.5)	–

Table 2: Averages and variances of climate covariates over different time periods. Averages are average values over the core areas. Core area values were the weighted averages according to GCM weights. Variances are average variances over the core areas. Core area variances were computed over the weighted averages of values for each core area.

GCM Scenario	Time Period	Avg. Precip. (mm)	Var. Precip.	Avg. Temp. (deg. C)	Var. Temp.
historical	Historical	2.027	0.007	11.483	0.456
ssp126	2020 - 2040	2.215	0.016	13.391	0.088
ssp126	2040 - 2060	2.276	0.016	13.989	0.080
ssp126	2060 - 2080	2.266	0.026	14.367	0.069
ssp126	2080 - 2100	2.280	0.013	14.020	0.089
ssp245	2020 - 2040	2.154	0.012	13.157	0.112
ssp245	2040 - 2060	2.229	0.019	14.070	0.236
ssp245	2060 - 2080	2.254	0.020	14.943	0.076
ssp245	2080 - 2100	2.267	0.023	15.419	0.041
ssp585	2020 - 2040	2.149	0.016	13.521	0.247
ssp585	2040 - 2060	2.202	0.012	14.920	0.430
ssp585	2060 - 2080	2.266	0.019	16.699	0.230
ssp585	2080 - 2100	2.284	0.018	18.014	0.229

Table 3: Results from colonization model for each core area. $\text{Pr}(\text{colonize} \mid \text{cover} = 0)$ reads, 'the probability of colonization given that current cover is zero.'

Core area	$\text{Pr}(\text{colonize} \mid \text{cover} = 0)$	Mean cover in colonized cells
Bear River	0.35	3
Blacks Fork	0.14	2
Buffalo	0.35	2
Continental Divide	0.22	2
Crowheart	0.21	2
Daniel	0.22	2
Douglas	0.37	2
Elk Basin East	0.42	2
Fontenelle	0.17	2
Grass Creek	0.15	2
Greater South Pass 1	0.17	2
Greater South Pass 2	0.14	2
Greater South Pass 3	0.18	2
Greater South Pass 4	0.23	2
Greater South Pass 5	0.13	2
Hanna	0.21	2
Heart Mountain	0.31	2
Hyattville	0.18	2
Jackson	0.42	4
Little Mountain	0.43	3
Natrona 1	0.21	2
Natrona 2	0.30	2
Natrona 3	0.19	2
Newcastle	0.19	2
North Gillette	0.17	2
North Glenrock	0.28	3
North Laramie	0.38	3
Oregon Basin	0.19	2
Salt Wells	0.20	2
Shell	0.19	2
South Rawlins	0.39	3
Thermopolis	0.26	3
Thunder Basin	0.24	2
Washakie	0.36	3

Table 4: LASSO-penalized coefficient values for the selected model for classifying temperature sensitivity. Note that all predictor values were averaged over grid cells within a core area and then averaged over depth from surface. The 'alpha' covariate is: 'scale parameter inversely proportional to mean pore diameter'. Standard errors, confidence intervals, and/or p-values are not reported because these metrics are not yet available for penalized regression under frequentist framework.

Soil property	LASSO-penalized coefficient value
95th percentile of alpha	0.15
95th percentile of clay percentage	0.34
5th percentile of saturated hydraulic conductivity	0.20
5th percentile of organic matter	0.30
5th percentile of sand percentage	0.22
95th percentile of sand percentage	0.48